AGU ADVANCING EARTH AND SPACE SCIENCE

Water Resources Research

RESEARCH ARTICLE
10.1029/2022WR032907

# A (Simplified) Biogeochemical Numerical Model to Predict Saturation, Porosity and Permeability During Microbially Induced Desaturation and Precipitation

**Liya Wang[1], Leon van Paassen[2], Vinh Pham[3], Nariman Mahabadi[4], Jia He[5], and Yunqi Gao[5]**

[1]Key Laboratory of Roads and Railway Engineering Safety Control (Shijiazhuang Tiedao University), Ministry of Education, Shijiazhuang, China, [2]School of Sustainable Engineering and the Built Environment, Arizona State University, Tempe, AZ, USA, [3]Division of Geotechnology, Thuyloi University, Hanoi, Vietnam, [4]Department of Civil Engineering, University of Akron, Akron, OH, USA, [5]Key Laboratory of Ministry of Education for Geomechanics and Embankment Engineering, Hohai University, Nanjing, China

**Abstract** Microbially Induced Desaturation and Precipitation (MIDP) through denitrification is an emerging ground improvement method in which indigenous nitrate reducing bacteria are stimulated to introduce biogas, biominerals and biomass in the soil matrix. In this study, a numerical model is developed to evaluate the effect of biogas, biominerals and biomass on the hydraulic properties of soils treated with MIDP. The proposed model couples the biochemical conversions to changes of porosity and water saturation and predicts changes in permeability through two separate power law equations. Experimental studies from the literature are used to calibrate the model. Comparing the results with other studies on bioclogging or biomineralization in porous media reveals that the combined production of biogas, biomass, and biominerals results in efficient clogging, in the sense that only a small amount of products leads to a substantial permeability reduction. Based on this comparison, the authors postulate that biogenic gas bubbles preferably form within the larger pore bodies. The presence of biogenic gas in the larger pore bodies forces calcium carbonate minerals and biomass to be formed mainly at the pore throats. The interaction between the different phases results in more efficient clogging than observed in other studies which focus on a single product only.

**Key Points:**

- A model predicts the combined effect of bioproducts on soil permeability treated by Microbially Induced Desaturation and Precipitation (MIDP)
- To simulate the permeability reduction by MIDP, the effects of the different products need to be treated separately
- The interaction between the different phases of products in MIDP may result in more efficient clogging than each single phase alone

**Supporting Information:**

Supporting Information may be found in the online version of this article.

**Correspondence to:**

Y. Gao,
yqgao89@hhu.edu.cn

**Citation:**

Wang, L., van Paassen, L., Pham, V., Mahabadi, N., He, J., & Gao, Y. (2023). A (simplified) biogeochemical numerical model to predict saturation, porosity and permeability during Microbially Induced Desaturation and Precipitation. *Water Resources Research*, *59*, e2022WR032907. https://doi.org/10.1029/2022WR032907

Received 27 MAY 2022
Accepted 24 DEC 2022

**Author Contributions:**

**Conceptualization:** Liya Wang, Leon van Paassen, Yunqi Gao
**Formal analysis:** Yunqi Gao
**Funding acquisition:** Liya Wang, Leon van Paassen, Jia He
**Investigation:** Liya Wang
**Methodology:** Liya Wang, Leon van Paassen
**Resources:** Liya Wang, Vinh Pham
**Supervision:** Leon van Paassen
**Validation:** Liya Wang
**Visualization:** Liya Wang, Nariman Mahabadi, Yunqi Gao
**Writing – original draft:** Liya Wang
**Writing – review & editing:** Leon van Paassen, Vinh Pham, Nariman Mahabadi, Jia He, Yunqi Gao



## 1. Introduction

Microbially Induced Desaturation and Precipitation (MIDP) via denitrification is being investigated for its potential as a novel bio-mediated ground improvement method to mitigate earthquake induced liquefaction (He et al., 2013, 2014; O'Donnell, 2016; O'Donnell, Kavazanjian, & Rittmann, 2017, O'Donnell, Rittmann, & Kavazanjian, 2017; Wang, Van Paassen, et al., 2020, Wang, Van Paassen, Gao, et al., 2020; Wu et al., 2018). By injecting a solution in the ground, which contains nitrate and dissolved organic carbon, nitrate reducing bacteria are stimulated to produce nitrogen gas and inorganic carbon. This catabolic redox reaction produces energy, which can be used by the nitrate reducing bacteria for growth and maintenance, while the nitrate and organic carbon can also serve as nitrogen and carbon source for cell synthesis. When providing nitrate and/or dissolved organic carbon as calcium salts (e.g., calcium nitrate and calcium acetate), the production of inorganic carbon results in the precipitation of calcium carbonate minerals.

The three main products of calcium-based denitrification, that is, biogenic gas bubbles (nitrogen and carbon dioxide), calcium carbonate minerals, and biomass, affect the soil properties and consequently change the soil behavior. The formation of gas bubbles desaturates the soil, increases the compressibility of the fluid, and reduces the buildup of excess pore pressures during undrained loading (He & Chu, 2014; Okamura & Noguchi, 2009; Okamura & Soga, 2006; O'Donnell, Kavazanjian, & Rittmann, 2017; Wang et al., 2021). Precipitation of calcium carbonate minerals can either cement the surface or the contact points of soil grains which affects the engineering properties of soil similar to Microbially Induced Carbonate Precipitation (MICP) by urea hydrolysis, that is, increasing the strength and stiffness of granular soils (DeJong et al., 2010, 2013; El Mountassir et al., 2018; Ivanov & Chu, 2008; Phillips et al., 2013; Whiffin et al., 2007). The increased strength through precipitation of biominerals also helps to increase the liquefaction resistance of loose granular soils (Gao et al., 2022; O'Donnell, Rittmann, & Kavazanjian, 2017; Wang, Van Paassen, Gao, et al., 2020; Wang et al., 2021).

However, gas bubbles and minerals fill the pore space and consequently can also affect the permeability of the soil. Soares et al. (1988, 1991) and Ronen et al. (1989) observed that desaturation through accumulation of entrapped gas formed by nitrate-reducing bacteria significantly reduces the hydraulic conductivity. However, when the gas is removed, the hydraulic conductivity can be recovered. To reduce the hydraulic conductivity through mineral precipitation, a significant amount of mineral precipitation is required. For example, Al Qabany and Soga (2013) and Dadda et al. (2017) showed when using MICP that more than 6% calcium carbonate was needed to reduce the permeability by one order of magnitude, which may be advantageous when applying MICP for bio-cementation as it allows substrates to be distributed over large distances, before significant clogging occurs (Whiffin et al., 2007). The third product of the denitrifying metabolism, biomass, also reduces hydraulic conductivity (Baveye et al., 1998; Cunningham et al., 1991; Thullner, 2010; Vandevivere, 1995; Vandevivere et al., 1995). As these biochemical conversions happen simultaneously in the aqueous state, changes in porosity, saturation and permeability, in turn, affect the flow field and consequent distribution of substrates and products of the biochemical processes. The interaction between the biochemical reactions and soil properties makes MIDP a complex coupled process.

This study aims to evaluate the permeability reduction during the MIDP process and develop a simplified zero-dimensional model for the porous media which couples the bio-chemical-physical processes in MIDP to changes in porosity, permeability, and saturation. Many models have been developed for MICP by urea hydrolysis at different scales and with varying levels of complexity (Cunningham et al., 2019; Ebigbo et al., 2012; Gai & Sánchez, 2019; Hommel et al., 2015; Minto et al., 2019; Qin et al., 2016; van Paassen, 2009; van Wijngaarden et al., 2011). Van Wijngaarden et al. (2011) built a model for MICP treated soil, which includes urea hydrolysis reaction, transportation of substrates, porosity changes caused by calcium carbonate precipitation and permeability reduction modeled with Kozeny-Carman relation. Later, van Wijngaarden et al. (2013) and van Wijngaarden et al. (2016) improved it by including the fixation and decay of bacteria. Martinez et al. (2014) adopted different rates to describe the urea hydrolysis and precipitation rate to model the concentrations of compounds and pH, neglecting the permeability changes. Ebigbo et al. (2012) included the precipitation kinetics in the model and two-phase flow when simulating the process using MICP to set up a hydraulic barrier for $CO_2$ storage site. Hommel et al. (2015) and Hommel et al. (2016) improved the model further by including bacteria transportation, complex solution chemistry, dissolution of calcite and the effects of biomass and calcite on porosity changes. Cuthbert et al. (2013), Qin et al. (2016), Nassar et al. (2018), Cunningham et al. (2019) and Minto et al. (2019) extended the model to simulate the field tests using MICP. For biomass clogging, Vandevivere et al. (1995) and Baveye et al. (1998) reviewed a lot of models which simulate the permeability reduction caused by biomass based on the Kozeny-Carman equations, most of which neglected the biomass growth. Ebigo et al. (2010) included the biofilm growth and its effect on permeability when simulating the biofilm and flow process in $CO_2$ storage reservoir. Hommel et al. (2018) summarized a lot of models which studies the porosity-permeability relations in MICP and biomass clogging.

Limited modeling efforts are reported so far on MIDP (O'Donnell et al., 2019; Pham, 2017). The models on MIDP mostly focused on the biochemical conversions but did not couple the products of the biochemical reactions to the resulting soil properties. O'Donnell et al. (2019) proposed an upgraded model by including intermediates, inhibition of microbes because of toxic intermediates, the chemical constituents and also considered various organic substrates in biochemical reactions, but pore-scale processes were ignored. The numerical model developed in this study, includes the metabolic (anabolic and catabolic) denitrification reactions, the formation of biogas, biominerals and biomass, and their effects on the degree of saturation, porosity, and permeability of the soil. A method to account for potential variations in the stoichiometry of the metabolic reaction is introduced and partial differential equations are used to describe changes in liquid fraction and porosity caused by the metabolic products (biogas, biomass, and biominerals). Finally, the changes in permeability were determined, considering the combined effects of biogas, biomass, and biominerals using two separate power law equations, which relate changes in degree of saturation and porosity to changes in permeability. Data from liquid batch experiments and column tests in modified triaxial test set-up were used to calibrate the model and fit the input parameters. Based on the combined experimental and numerical simulation results, the interaction between biogas, biominerals and biomass in the evolution of the pore space and permeability reduction are discussed.

## 2. Theory

The model considers the metabolic denitrification process in MIDP which produce biomass, biogas, and biomineral. The multicomponent bio-chemical process in porous media with changes in porosity, water saturation and permeability make the biogeochemical process of MIDP extremely complex. Our study mainly focuses on the (combined) effects of biogas, biomass, and biomineral on soil permeability. So, some assumptions were made to simplify the model.

1. The metabolic reaction of denitrification is split in a catabolic and an anabolic reaction, which is combined with a factor, $f_{cat,}$ as explain after. Bacteria decay and transportation are not considered.
2. The reaction rate is assumed to follow the Mond equation considering no inhibition.
3. The dry biomass density which is dry biomass per unit wet biomass volume is assumed to be constant at 50 kg/m$^3$.
4. The pH is buffered and remains around neutral as Pham, Nakano, et al. (2018) and Wang, Van Paassen, Gao, et al. (2020) showed.
5. The precipitation happens simultaneously with denitrification.
6. All produced DIC will either precipitate with calcium or leave the solution as carbon dioxide gas.
7. A zero-dimensional approach is used to describe the average concentration of calcium and nitrate in the liquid batch, and the average porosity, water saturation and permeability throughout the unit soil column.
8. The nucleation and growth kinetics of gas bubbles and biominerals are ignored. The capillary pressure is ignored, so the gas pressure is assumed to be equal to the water pressure.
9. The viscosity is constant, and the permeability is isotropic.
10. The changes in permeability were determined, considering the combined effects of biogas, biomass and biominerals using two separate laws, which relate changes in the degree of saturation and porosity to changes in permeability.

### 2.1. Biochemical Reactions

In the denitrification process, nitrate is stepwise reduced to nitrogen gas, while a source of organic carbon is oxidized to inorganic carbon. When providing calcium acetate and calcium nitrate as the main substrates, acetate acts as the carbon source and electron donor. The metabolic reaction can be split in a catabolic and an anabolic reaction. The catabolic reaction of the denitrification process can be expressed (per unit of acetate) in a single reaction equation using (Thomsen et al., 1994):

$$CH_3COO^- + 1.6NO_3^- + 0.6\,H^+ \xrightarrow{\text{bacteria}} 0.8N_2\uparrow + 2HCO_3^- + 0.8H_2O \quad (1)$$

The catabolic reaction generates the energy used in the anabolic reaction, in which biomass is produced. Hoh and Cord-Ruwisch (1997) and Şengör et al. (2013) recommended that it is necessary to include growth and maintenance energy thermodynamics via ATP/ADP cycling when model biosystems. Using $CH_{1.8}O_{0.5}N_{0.2}$ as the molecular formula for biomass, the anabolic reaction (per unit of biomass) is described as (Heijnen & Kleerebezem, 2009; Pham, Nakano, et al., 2018):

$$0.725CH_3COO^- + 0.2NO_3^- + 0.475H^+ \rightarrow CH_{1.8}O_{0.5}N_{0.2} + 0.45HCO_3^- + 0.2H_2O \quad (2)$$

Both Equations 1 and 2 are valid for a pH around neutral. Depending on the pH, dissolved inorganic carbon (DIC) can take the form of carbonate ($CO_3^{2-}$), bicarbonate ($HCO_3^-$) or carbonic acid ($H_2CO_3$). For a pH around seven bicarbonate ($HCO_3^-$) is the dominant species of DIC. The equations illustrate that at neutral pH both the anabolic and catabolic reactions consume protons, and thereby cause the pH to increase. The overall metabolic reaction can be determined by combining the catabolic and anabolic equation. The ratio at which these reactions are combined depends on the growth rate of the bacteria and can be described using the factor, $f_{cat}$, which defines how many catabolic reactions (per unit of carbon donor) are needed to generate sufficient energy for the growth and maintenance of one unit of biomass. Following this definition, the stoichiometric metabolic yield coefficient, $Y^m$, of each substrate and product can be calculated using (Heijnen & Kleerebezem, 2009):

$$Y^m = Y^a + f_{cat} \cdot Y^c \quad (3)$$

where $Y^a$ is the anabolic yield coefficient and $Y^c$ is the catabolic yield coefficient.

**Table 1**
*The Stoichiometric Coefficients, $Y^m$, of the Substrates and Products in the Metabolic Denitrification Reaction for the Equilibrium Speciation Reactions per C-Mol of Biomass*

| Species | Stoichiometric coefficients denitrification reaction | Stoichiometric coefficients precipitation and gas formation reactions |
|---|---|---|
| $CH_3COO^-$ | $-0.725 - f_{cat}$ | |
| $HCO_3^-$ | $0.45 + 2f_{cat}$ | $-0.45 - 2f_{cat}$ |
| $NO_3^-$ | $-0.2 - 1.6f_{cat}$ | |
| $H^+$ | $-0.475 - 0.6f_{cat}$ | $0.475 + 0.6f_{cat}$ |
| $N_2$ | $0.8f_{cat}$ | |
| $H_2O$ | $0.2 + 0.8f_{cat}$ | $-0.0125 + 0.7f_{cat}$ |
| $CH_{1.8}O_{0.5}N_{0.2}$ | 1 | |
| $Ca^{2+}$ | | $-0.4625 - 1.3f_{cat}$ |
| $CaCO_3$ | | $0.4625 + 1.3f_{cat}$ |
| $CO_2$ | | $-0.0125 + 0.7f_{cat}$ |

Combining Equations 1 and 2 using $f_{cat}$, the stoichiometric coefficient of the main species involved in the metabolic denitrification reaction can be determined as listed in Table 1. The minimum value for $f_{cat}$ is 0.487, which can be derived based on the required energy for biomass growth and maintenance following Heijnen and Kleerebezem (2009) and corresponds to maximum growth rate conditions. If biomass growth is completely inhibited and the microbial cells continue to respire for maintenance only, $f_{cat}$ would be equal to infinity.

In the presence of dissolved calcium, the production of DIC may cause precipitation of calcium carbonate minerals. At neutral pH the precipitation reaction can be described as follows:

$$Ca^{2+} + HCO_3^- \rightleftharpoons Ca^{2+} + CO_3^{2-} + H^+ \rightleftharpoons CaCO_3 \downarrow + H^+ \quad (4)$$

The precipitation reaction releases a proton. At the same time some of the produced bicarbonate may also associate with protons to from carbonic acid, which in turn may dissociate and transfer to the gas phase as carbon dioxide gas.

$$HCO_3^- + H^+ \rightleftharpoons H_2CO_3 \rightleftharpoons CO_2 \uparrow + H_2O \quad (5)$$

Through the combined processes of denitrification, precipitation of calcium carbonate and exsolution of carbon dioxide gas, the pH is buffered and remains around neutral (between 6 and 8) during the entire MIDP process as demonstrated by Pham, Nakano, et al. (2018), Pham, Van Paassen, Van der Star, et al. (2018) and Wang, Van Paassen, Gao, et al. (2020). Considering that the pH is buffered and remains around neutral and that the water which is used to prepare the substrate solutions (e.g., tap water, recycled groundwater or surface water) often already contains DIC and calcium through contact with the atmosphere and surrounding environment, the different biochemical reactions can be combined and simplified, by assuming all produced DIC will either precipitate as calcium carbonate or leave the solution as carbon dioxide gas. Combining Equations 1–5, we can determine the yield coefficients as shown in Table 1, for: (a) calcium, which is half of the sum of the yield coefficients for acetate and nitrate; (b) calcium carbonate, which is the opposite of the yield coefficient for calcium, that is, calcium consumption is equal to calcium carbonate production; (c) carbon dioxide, which is the difference between the amount of bicarbonate produced in the denitrification reaction and the bicarbonate consumed by $CaCO_3$ precipitation; (d) bicarbonate and protons, which are the opposite in the combined precipitation and gas formation reactions, which means there is no net change in bicarbonate and proton concentration and consequent pH or alkalinity. Combining all processes, the metabolic reaction can be rewritten in a single equation, in which the stoichiometry only depends on the biomass growth rate, that is, the value for $f_{cat}$, which is illustrated in Figure 1.

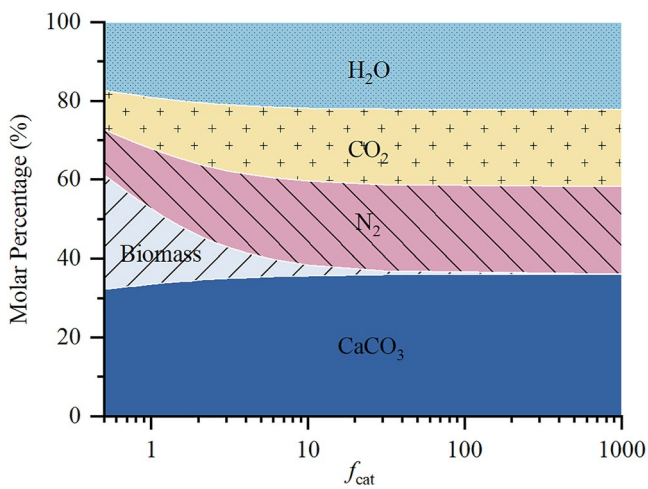


**Figure 1.** Relative molar percentage of products as a function of stoichiometric factor $f_{cat}$.

The catabolic reaction, which corresponds to the metabolic reaction when there is no biomass growth ($f_{cat} \rightarrow \infty$), normalized per mol of acetate, becomes:

$$Ca(C_2H_3O_2)_2 + 1.6Ca(NO_3)_2 \rightarrow 1.6N_2 + 2.6CaCO_3 + 1.4CO_2 + 3H_2O \quad (6)$$

While the metabolic reaction at maximum growth rate ($f_{cat} = 0.487$), normalized per mol of acetate, becomes:

$$Ca(C_2H_3O_2)_2 + 0.82Ca(NO_3)_2 \rightarrow 1.62CH_{1.8}O_{0.5}N_{0.2} + 1.82CaCO_3 + 0.66N_2 + 0.56CO_2 + 1.54H_2O \quad (7)$$

The actual metabolic stoichiometry during the MIDP process may vary between the conditions of zero and maximum growth and can be determined after treatment based on the measurement of residual substrate concentrations (Pham, 2017).

The kinetics of the coupled reaction equation can be described using a Monod kinetic equation (Doran, 2013) which suggests that the reaction rate follows

a first order equation at low substrate concentrations, but reaches a constant maximum value at high substrate concentrations:

$$\frac{\partial C_i}{\partial t} = r = r_0 \cdot Y_i^{\mathrm{m}} C_{\mathrm{biomass}} \cdot \frac{C_{\mathrm{CH_3COO^-}}}{K_{\mathrm{m1}} + C_{\mathrm{CH_3COO^-}}} \cdot \frac{C_{\mathrm{NO_3^-}}}{K_{\mathrm{m2}} + C_{\mathrm{NO_3^-}}} \tag{8}$$

where $r_0$ (mol substrate/C-mol biomass/s) is the specific uptake rate for one mole of biomass, $C_i$ and $Y_i^{\mathrm{m}}$ are the concentration and yield coefficient of component $i$, $C_{\mathrm{biomass}}$, $C_{\mathrm{CH\ 3COO}^-}$, and $C_{\mathrm{NO_3^-}}$ are the concentrations of biomass, acetate, and nitrate, and $K_{\mathrm{m1}}$ and $K_{\mathrm{m2}}$ are the affinity constant for acetate and nitrate, respectively, 0.06 kmol/m$^3$. Note that in case of zero growth, the denitrification only includes catabolic reaction as shown in Equation 6. The reaction rate then only depends on the initial microbe concentration and the specific uptake rate.

### 2.2. Porosity, Permeability, and Saturation Relationships

Calcium carbonate precipitation and the formation of biomass and/or biogenic gas reduce the permeability of the soil. However, the mechanism by which they reduce the permeability is different (Brooks & Corey, 1964; Ghezzehei et al., 2007; Hommel et al., 2018; Ippisch et al., 2006; Mualem, 1976; Stone, 1970; Thullner, 2010; van Genuchten, 1980). Many kinds of equations are used describe the effects of saturation, like van Genuchten equation, Brooks equation and power law while power law is commonly used to describe the porosity effects. In this study, the permeability change observed during separate MIDP experiments is analyzed using two relationships: one which relates permeability to porosity and one which relates permeability to the degree of water saturation.

#### 2.2.1. Porosity-Permeability Relationship

Mineral precipitation and biomass formation in porous media fill the pore space, reducing the pore size and the porosity. A reduction in porosity or mean pore size causes the water permeability to decrease. Various relationships have been developed which relate changes in porosity to changes in permeability. Some are based on physical principles, with varying assumptions, others are just fitted to empirical data for various experimental conditions (Hommel et al., 2018; Thullner, 2010). One of these relationships, which has been commonly used in literature is the power law (Ives & Pienvichitr, 1965). In this study a modified form of the power law (Verma & Pruess, 1988) is used:

$$k_{r\theta} = \frac{k_{\mathrm{s}}}{k_0} = \left(\frac{\theta - \theta_{\mathrm{cr}}}{\theta_0 - \theta_{\mathrm{cr}}}\right)^{\eta} \tag{9}$$

where $k_{r\theta}$ is the relative change in permeability due to changes in porosity, $k_{\mathrm{s}}$ and $k_0$ are the current and initial saturated permeability, respectively, $\theta$ and $\theta_0$ are the current and initial porosity, $\theta_{cr}$ is a critical porosity at which the permeability terminates, and $\eta$ is an empirical constant, which is fitted to the experimental data. In our model we assume $\theta_{\mathrm{cr}}$ is zero. The empirical constant $\eta$ can vary significantly, depending on the process causing the change in permeability. For example, reported values range from $\eta = 2.5$–3 for plastic deformation of the solid phase, to $\eta = 8$ for chemical precipitation, $\eta \geq 10$ for chemical alteration, and $\eta \geq 20$ for dissolution in limestone (Bernabé et al., 2003; Hommel et al., 2018).

Assuming biominerals and biomass itself have negligible porosity (thus water cannot percolate through them) and are not transported with the fluid flow, changes in porosity $\theta$ can be directly related to changes in the concentrations of produced biomass and calcium carbonate resulting from the biochemical reaction and can be described using:

$$\frac{\partial \theta}{\partial t} = -\frac{\partial \left(C_{\mathrm{CaCO_3}} \theta_l\right)}{\partial t} \frac{M_{\mathrm{CaCO_3}}}{\rho_{\mathrm{CaCO_3}}} - \frac{\partial (C_{\mathrm{biomass}} \theta_l)}{\partial t} \frac{M_{\mathrm{biomass}}}{\rho_{\mathrm{biomass}}} \tag{10}$$

where $\partial C_{\mathrm{CaCO3}}/\partial t$ is the change in calcium carbonate concentration in time, which follows the overall biochemical reaction; $M_{\mathrm{CaCO3}}$, the molar weight of calcium carbonate is 100 g/mol; $\rho_{\mathrm{CaCO3}}$, the density of calcium carbonate (calcite) is 2,710 kg/m$^3$; $M_{\mathrm{biomass}}$, the molar weight of biomass, which considering $CH_{1.8}O_{0.5}N_{0.2}$ as the molecular formula for biomass is 24.6 g/C-mol; $\rho_{\mathrm{biomass}}$ is the dry biomass density, which is the dry mass of biomass per unit volume of wet biomass, and the volume of wet biomass is the volume of dry biomass and interstitial water. The

dry biomass density is found to vary between 20 and 120 kg/m$^3$ (Chen & Chen, 2000; Ohashi & Harada, 1994; Rabah & Dahab, 2004; Ro & Neethling, 1991; Zhan et al., 2006) where the biomass density decreased with increasing biofilm thickness. Considering the confined space in the pores between the sand grains, it is expected the biomass density will be in the higher end of this range. For the model we assumed a biomass density of 50 kg/m$^3$; $\partial C_{\text{biomass}}/\partial t$ is the change in biomass concentration; and $\theta_l$ is the liquid fraction of the pores or the volumetric water content, that is, the ratio between the volume of water and the total soil volume. The initial value for porosity of the soil before treatment should be corrected for the initial volume of biomass.

### 2.2.2. Saturation-Permeability Relationship

The presence of biogas in the pore fluid reduces the degree of (water) saturation, which consequently reduces the permeability. The permeability of a partially saturated soil, $k$, can be obtained using:

$$k = k_{\text{rs}} \cdot k_{\text{s}} \tag{11}$$

where $k_{\text{rs}}$ is the relative change in permeability as a result of change in saturation and $k_{\text{s}}$ is the permeability under saturated conditions. Similar as for biomass and biomineral formation, various empirical equations have been established which relate the relative permeability to changes in the water saturation, for example, van Genuchten, Brooks and Corey, or Stone equations (Brooks & Corey, 1964; Stone, 1970; van Genuchten, 1980). In this study, a modified version of Stone equation (Mahabadi & Jang, 2014) is used to describe the relationship between saturation and the relative water permeability:

$$k_{\text{rs}} = {S_{\text{e}}}^n = \left(\frac{\theta_l - \theta_{\text{r}}}{\theta_{\text{s}} - \theta_{\text{r}}}\right)^n = \left(\frac{S_{\text{w}} - S_{\text{r}}}{1 - S_{\text{r}}}\right)^n \tag{12}$$

where $S_{\text{e}}$ is the effective saturation, $\theta_l$, is the liquid fraction of the pores or the volumetric water content, $\theta_{\text{r}}$ is the residual volumetric water content, $\theta_{\text{s}}$ is the fully saturated volumetric water content (which equals to porosity $\theta$ corrected for initial biomass concentration), $S_{\text{w}}$ is the water saturation; $S_{\text{r}}$ is the residual water saturation, and $n$ is the exponent which may vary for different pore size distributions or gas distributions, which can be fitted to the observed data (Mahabadi & Jang, 2014). Following van Genuchten (1980), the value of $n$ can be determined from the soil water retention curve (SWRC).

The volume of biogenically produced gas and consequent changes in water saturation depends on several factors, including (a) the yield coefficient of nitrogen and carbon dioxide in the biochemical reaction, which defines how much moles of gas are produced in time, (b) the gas pressure, which affects the solubility of the gas according to Henry's law and relates the amount of moles of gas to its volume following the ideal gas law, and (c) the ability of the gas to migrate (van Paassen et al., 2018). When the gas is entrapped (or occluded), the gas pressure, $p_{\text{g}}$, can be estimated using the Young-Laplace equation:

$$p_{\text{g}} = p_{\text{atm}} + p_{\text{w}} + p_{\text{c}} = p_{\text{atm}} + p_{\text{w}} + \frac{2\gamma}{R_{\text{b}}} \tag{13}$$

where $p_{\text{atm}}$ is the atmospheric pressure (±101 kPa or 1 atm); $p_{\text{w}}$ is the water pressure which is the sum of the hydrostatic and excess pore water pressure (similar to back pressure in the triaxial cell), and $p_{\text{c}}$ is the capillary pressure, which is a function of the water surface tension $\gamma$ (±0.072 N/m) and the gas bubble radius $R_{\text{b}}$. The bubble radius depends on the pore size distribution. Gas prefers to fill up the large pores first before filling or migrating through the smaller pore throats. The capillary pressure can be estimated based on the pore (or soil grain-) size distribution or SWRC curve (van Paassen et al., 2018).

Ignoring nucleation and growth kinetics of gas bubbles, gas formation is assumed to start when the dissolved concentration exceeds the solubility. The change in liquid fraction due to nitrogen gas production can then be described as follows:

$$\begin{cases} \dfrac{\partial \theta_{l,\text{N}_2}}{\partial t} = 0 & if\ C_{\text{N}_2} \le C^*_{\text{N}_2} = H^{cp}_{\text{N}_2} p_{\text{N}_2} \\ \dfrac{\partial \theta_{l,\text{N}_2}}{\partial t} = \dfrac{-\partial\left(C_{\text{N}_2}\theta_l\right)}{\partial t}\dfrac{RT}{p_g} & if\ C_{\text{N}_2} > C^*_{\text{N}_2} \end{cases} \tag{14}$$

where $p_{\text{N}_2}$ is the partial pressure of nitrogen in the gas phase, $R$ is the gas constant, 8.314 m$^3 \cdot$ Pa $\cdot$ K$^{-1} \cdot$ mol$^{-1}$; $T$ is the temperature in K, and $H^{cp}_{\text{N}_2}$ is Henry's constant for nitrogen gas, $6.1 \times 10^{-4}$ mol $\cdot$ L$^{-1} \cdot$ atm$^{-1}$.

Following the same procedure, the change in liquid fraction due to exsolution of carbon dioxide is:

$$\begin{cases} \dfrac{\partial \theta_{l_{CO_2}}}{\partial t} = 0 & if\ C_{CO_2} \le C^*_{CO_2} = H^{cp}_{CO_2} p_{CO_2} \\ \dfrac{\partial \theta_{l_{CO_2}}}{\partial t} = -\dfrac{\partial \left(C_{CO_2} \theta_l\right)}{\partial t} \dfrac{RT}{p_g} & if\ C_{CO_2} > C^*_{CO_2} \end{cases} \tag{15}$$

where $H^{cp}_{CO_2}$ is Henry's constant for carbon dioxide, $3.4 \times 10^{-2}$ mol/(L · atm).

The liquid fraction can be reduced due to gas formation, until the degree of saturation drops below a certain threshold at which the gas forms a continuous pathway and starts to percolate. Further production of the nitrogen gas cannot push more liquid out from the soil and the saturation will not be reduced further although the reaction may continue. Here this percolation threshold saturation, $S_v$, is defined as the liquid saturation at which a continuum gas-phase is formed, which allows the gas to escape from the pore space (Sahimi, 1993). Pham, Van Paassen, and Van der Star (2018) performed several laboratory tests on sand columns with varying grain size distribution and pressure conditions and found that such a threshold exists at a degree of saturation around 75%–85%. In natural sediments it may be difficult to get a precise value for $S_v$, due to the heterogeneity of the pore structure. For example, in a sandy-silt stratified soil system this threshold may be higher as silt lenses can prevent upward migration of gas and cause the gas phase to spread laterally (Stallings Young et al., 2021). Thus, the change in liquid fraction is described using:

$$\begin{cases} \dfrac{\partial \theta_l}{\partial t} = \dfrac{\partial \theta_{l_{N_2}}}{\partial t} + \dfrac{\partial \theta_{l_{CO_2}}}{\partial t}, & if\ \theta_l \le \theta \cdot S_v \\ \dfrac{\partial \theta_l}{\partial t} = 0 & if\ \theta_l = \theta \cdot S_v \end{cases} \tag{16}$$

Using this model, the concentration of chemical species, porosity, saturation, and the permeability can be predicted for different treatment strategies and soil conditions. However, the model is built based on various assumptions and requires fitting of several parameters, such as the initial biomass concentration and constants $f_{cat}$, $\theta_{cr}$, $n$, and $\eta$. Some of these parameters may be estimated from empirical correlations or lab characterization or literature values. However, the presence of gas may affect the location where calcium carbonate and biomass are formed. It is still unclear how the simultaneous formation of biogas, biomass and biominerals during MIDP will affect the porosity-permeability relationships. Therefore, calibration of the model is required. To this end, the model has been used to simulate the results of liquid batch tests and soil column tests that were reported in the literature. Experimental details and results of these experiments are presented in the following section.

## 3. Results and Analysis

### 3.1. Liquid Batch Conditions

MIDP experiments in liquid batch conditions were reported by Pham, Van Paassen, Van der Star, et al. (2018), O'Donnell, Kavazanjian, and Rittmann (2017), and Wang, Van Paassen, Gao, et al. (2020). Here the experiments reported by Wang, Van Paassen, Gao, et al. (2020) were used to calibrate the model for liquid batch conditions. In this experiment a liquid medium containing 25 mmol/L calcium nitrate and 25 mmol/L calcium acetate was inoculated with a mixed enrichment culture of nitrate-reducing bacteria from one of the earlier cultivations and the nitrate and calcium concentrations were monitored in time. COMSOL Multiphysics was used in the simulation of the liquid batch test. The specific uptake rate $r_0$, $K_{m1}$, and $K_{m2}$, initial biomass concentration and $f_{cat}$ were calibrated to fit the model to the measured concentration of nitrate through trial and error. The results are shown in Figure 2. The solid blue line shows the simulated nitrate and calcium concentration assuming zero biomass growth (catabolic conditions). The dashed green line in Figure 2a shows the best fit between measured and simulated nitrate concentrations, which was obtained with $r_0$ at $1.65 \times 10^{-4}$ mol-acetate/mol-biomass/s, $K_{m1}$ and $K_{m2}$ at 0.06 kmol/m$^3$, an initial concentration of biomass of 0.68 mol/m$^3$ and $f_{cat}$ at 3.

Using the same values for the fitting parameters to simulate the calcium concentration (Figure 2b), showed that final calcium concentration fitted well, but the simulated calcium consumption was faster than measured. The delay in calcium consumption could be partly attributed to the fact that nucleation and growth kinetics of calcium carbonate precipitation and gas transfer limitations were ignored in the simplified model. The results indicated

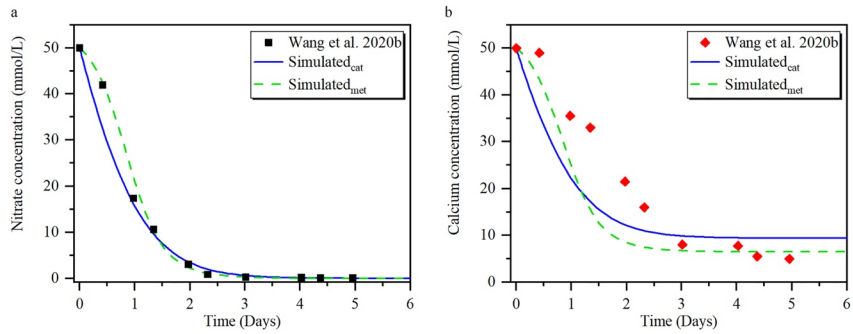


**Figure 2.** Measured and simulated nitrate (a) and calcium (b) concentrations based on experimental data from Wang, Van Paassen, Gao, et al. (2020).

that simulation considering the biomass growth is more closed to the experimental data. The value of $f_{cat}$ can be well fitted on the residual substrate concentrations (acetate, nitrate and/or calcium), which can be measured directly or indirectly using a correlation with electrical conductivity (Zeng et al., 2021).

### 3.2. Sand Column Tests

Sand column tests on MIDP were performed by O'Donnell, Kavazanjian, and Rittmann (2017), Pham, Van Paassen, Van der Star, et al. (2018), van Paassen et al. (2010), Wang, Van Paassen, et al. (2020), Wang, Van Paassen, Gao, et al. (2020), (Wang et al., 2021) for varying sand types and pressure conditions. Selected results from these studies were used to test the model.

Figure 3 presents the measured saturation during one of the sand column tests performed by Wang, Van Paassen, Gao, et al. (2020). In this experiment, a sand column was treated in a modified triaxial cell. The sample was placed at 100 kPa pore pressure and 171 kPa confining pressure, which correspond to hydrostatic stress conditions at approximately 10 m below surface and groundwater level. Consequently, the column was injected with a substrate solution containing 25 mmol/L calcium acetate, 25 mmol/L calcium nitrate, which was inoculated with a mixed culture of denitrifying micro-organisms. Similar to the batch liquid experiments, the numerical simulation was able to capture the desaturation trend. A specific uptake rate $r_0$ of $0.9 \times 10^{-4}$ mol-substrate/mol biomass/s, initial concentration of biomass of 0.1 mol/m$^3$ and $f_{cat}$ of three were found to be the best fit to calibrate the simulations to the measured results. The degree of saturation reached a minimum value of 0.75 after 5 days, similar to the expected value based on full conversion of substrates. Deviations between the measured and simulated degree of saturation may be due to the fact the kinetics of gas nucleation was ignored in the simplified model. After the lowest saturation was reached, the degree of saturation gradually increased back to 0.82, which was not captured by the simulation. The saturation recovery after day 5–6 could either be attributed to dissolution of carbon dioxide and nitrogen gas and diffusion through the membrane as suggested by Pham, Van Paassen, Van der Star, et al. (2018) or may be due to venting of gas out of the cell. Dissolution of gas transfers the volume of the gas phase to aqueous state, but the total amount of gas doesn't change for the sample. Venting gas only changes the amount of soil sample but not the backpressure system while diffusion through membrane changes it in the backpressure system. The percolation threshold saturation was not defined by Wang, Van Paassen, Gao, et al. (2020), but other tests (Pham, Van Paassen, & Van der Star, 2018; Stallings Young et al., 2021) reported the water saturation at which gas started to migrate and no further desaturation was obtained, ranging between 50% and 80%.

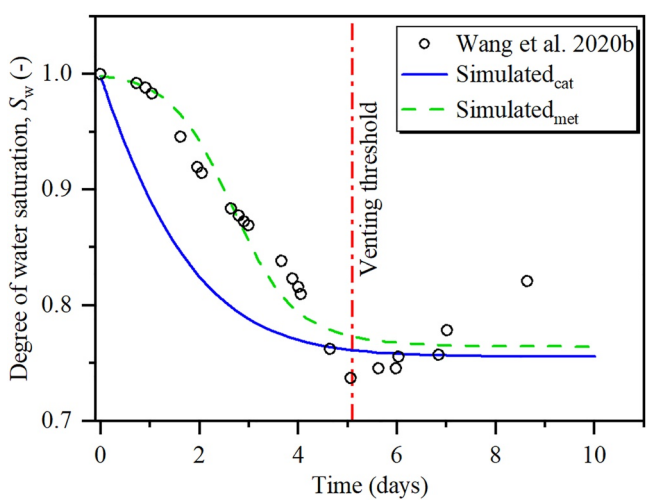


**Figure 3.** Saturation development in the triaxial specimen under 100 kPa pore pressure and 171 kPa confining pressure based on experimental data from Wang, Van Paassen, Gao, et al. (2020).

Both the experiments of Pham, Van Paassen, Van der Star, et al. (2018) and Wang, Van Paassen, et al. (2020) were used to study the effect of simultaneous formation of biogas, biominerals, and biomass on the permeability in sand columns exposed to multiple MIDP treatment cycles (Figure 4). Pham, Van Paassen, Van der Star, et al. (2018) performed sand column tests in a

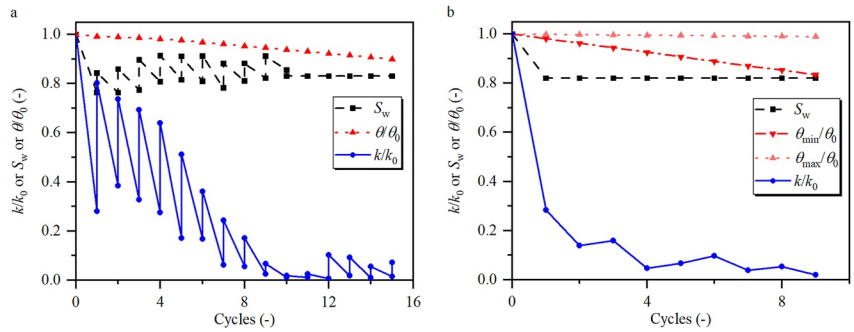


**Figure 4.** Relative change in hydraulic conductivity, $k/k_0$, water saturation, $S_w$, and porosity, $\theta/\theta_0$ after Pham, Van Paassen, Van der Star, et al. (2018) (a) and Wang, Van Paassen, et al. (2020) (b).

modified triaxial cell at 200 kPa cell pressure and 100 kPa pore pressure in which a fine poorly graded sand ($d_{50}$: 0.138 mm) was flushed with 15 cycles of injection with substrate solution containing 12 mmol/L calcium acetate and 10 mmol/L calcium nitrate (Figure 4a). They observed that during the reaction phase of each cycle, water was expelled from the sand sample due to the formation of biogenic gas, which reduced the water saturation and consequently would reduce the hydraulic conductivity. The water saturation did not fall below 75%–80%, which was interpreted as the percolation threshold saturation, $S_v$, at which a continuous gas phase was formed, and the gas starts percolating upwards. Further gas generation did not affect the saturation anymore. During each flushing phase some of the entrapped gas was removed, which consequently led to a partial recovery of the hydraulic conductivity. As a result, after multiple treatment cycles both the water saturation and hydraulic conductivity shows a fluctuating pattern, relatively immediately after the reaction phase and increasing during the flushing phase. In this case, water saturation fluctuates between 75% and 91% around an average value for $S_v$ of 0.82. In general, hydraulic conductivity decreased as the number of cycles increased, while at the 11th cycle hydraulic conductivity is almost reduced to zero, which presents a complete clogging. The clogging was partly removed by increasing the hydraulic gradient, after which the hydraulic conductivity partly recovered. Subsequent flushes were injected at a higher hydraulic gradient. Assuming the water saturation did not decrease below the percolation threshold saturation, the decreasing trend in hydraulic conductivity after multiple treatment cycles was attributed to the formation and accumulation of biomass and calcium carbonate. From the concentrations of residual acetate and nitrate in the effluent that were measured by Pham, Van Paassen, Van der Star, et al. (2018), the stoichiometry factor, $f_{cat}$, of the metabolic reaction was calculated for each cycle and the amount of biomass and calcium carbonate were determined. From the calculated amount of biomass and calcium carbonate, the change in porosity was calculated using Equation 10. The resulting porosity change by calcium carbonate precipitation after 15 cycles was still very negligible (only 0.9%). The calculated porosity reduction due to the formation of biomass was more significant, which was about 9% after 15 cycles when assuming the value for dry biomass density, $\rho_b$, is 50 kg/m$^3$. The value of $f_{cat}$, the total amount of calcium carbonate and dry biomass, and the resulting porosity reductions are listed in Supporting Information S1.

Wang, Van Paassen, et al. (2020) performed similar column experiments in a modified triaxial test set-up on a slightly coarser poorly graded sand ($d_{50}$: 0.2 mm) at 171 kPa cell pressure and 100 kPa pore pressure with 3, 6, and 9 cycles of injection of substrate solution containing 25 mmol/L calcium acetate and 25 mmol/L calcium nitrate. The study shows significant clogging up to three orders of magnitude within 4–9 flushes where part of the clogging was recovered by building up the hydraulic head. Wang, Van Paassen, et al. (2020) did not report any residual concentrations in the expelled liquid, or a degree in saturation during the different flushes. However, using the model, the minimum and maximum amounts of biomass and calcium carbonate and consequent porosity reduction can still be calculated, assuming the value for $f_{cat}$ ranging between maximum growth (0.487) and zero growth ($\infty$), $\rho_{biomass}$ at 50 kg m$^{-3}$ and a constant value for $S_v$ after the first flush at 0.82. The results are shown in Figure 4b, and the data is provided in Supporting Information S1.

## 4. Discussion

Power law Equations 9 and 12 are used to investigate how the MIDP process affects the saturation- and porosity-permeability relationships. The simulation results via the proposed coupled biogeochemical model

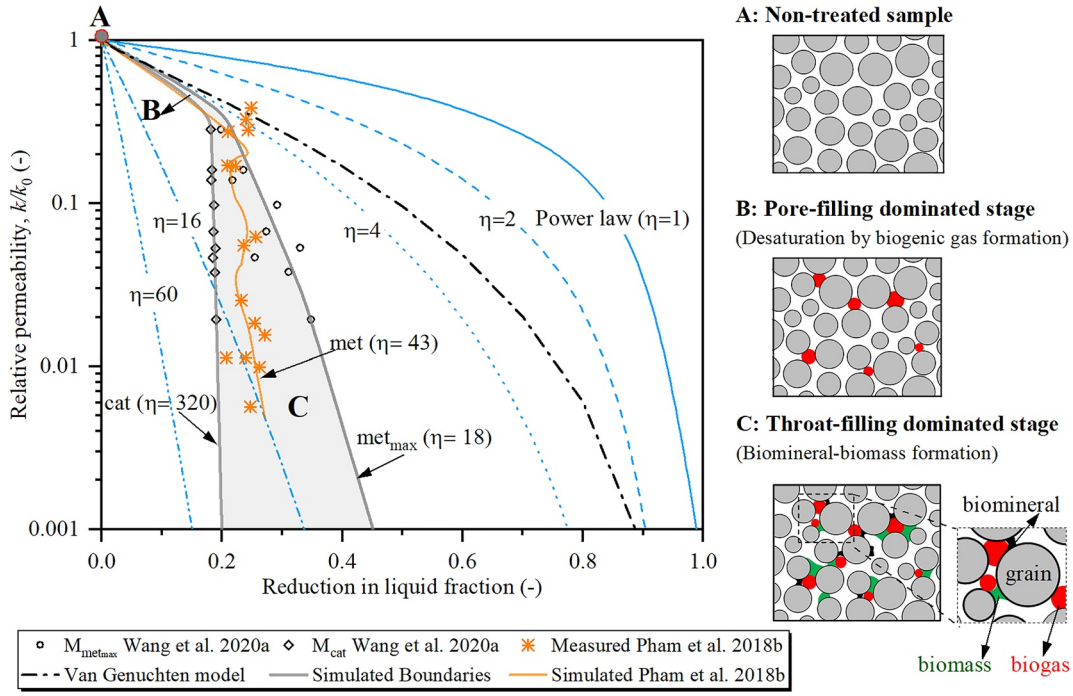


**Figure 5.** Measured and simulated relationships between the reduction in liquid fraction and relative permeability based on the data from the two studies by Pham, Van Paassen, Van der Star, et al. (2018) and Wang, Van Paassen, et al. (2020). The blue lines show the simulated permeability using a single power law (Equation 9) for different values for fitting parameter $\eta$, the black dash-dotted line shows the saturation-permeability relationship calculated using Van Genuchten equation which was fitted on the measured SWRC for the sand used by Wang, Van Paassen, et al. (2020) (see Supporting Information S1). Three different stages in the development of permeability are identified.

using Wang, Van Paassen, et al. (2020) and Pham, Van Paassen, Van der Star, et al. (2018) and the experimental results are presented in Figure 5. To illustrate the combined effect of saturation and porosity, which change simultaneously during MIDP, the permeability is plotted as a function of the reduction of the liquid fraction of the pore space, which corresponds to the mobile porosity or the pore volume in which the liquid fraction can flow. The blue lines in Figure 5 show the predicted permeability change as a function of porosity or water saturation using a single power law Equation 9 with varying fitting parameters $\eta$. The measured and calculated data points based on the experimental data suggest that the permeability reduction during multiple cycles of MIDP treatment cannot be fully described with a single power law equation. Instead, the effect of desaturation by biogenic gas formation and the impact of porosity reduction as a result of the accumulation of calcium carbonate minerals and biomass need to be separated, each described with a different power law relationship.

During the first treatment cycle, the amount of biomass and biominerals that was formed was still relatively low and the reduction in permeability could mainly be attributed to the effect of desaturation. As in this stage the dominating process is desaturation, we can assume that the reduction in liquid fraction ($x$-axis of Figure 5) is equal to the reduction in water saturation. Therefore, a two-phase permeability relation (saturation-relative permeability) like Van Genuchten (1980) or the one-phase power law relation (Equation 12) can be used to find the best empirical fit to the measured data points. It was found that using a factor $n$ of 3 provides a good fit between measured and simulated permeability reduction using both single-phase power law and two-phase van Genuchten relations.

Following by subsequent treatment cycles, accumulation of biomass and biominerals dominates the clogging mechanism. A significant permeability reduction is achieved by a relatively small accumulation of biomass and biominerals, while the reduction of water saturation is limited. Consequently, the permeability reduction could not be described using a single power law for the entire MIDP process. While the factor $n$ that was fitted to relate the water saturation to the permeability constant at 3, the fitting factor $\eta$ for the second power-law that describes the porosity-permeability relationship (Equation 9) was estimated to range between 18 and 320 depending on

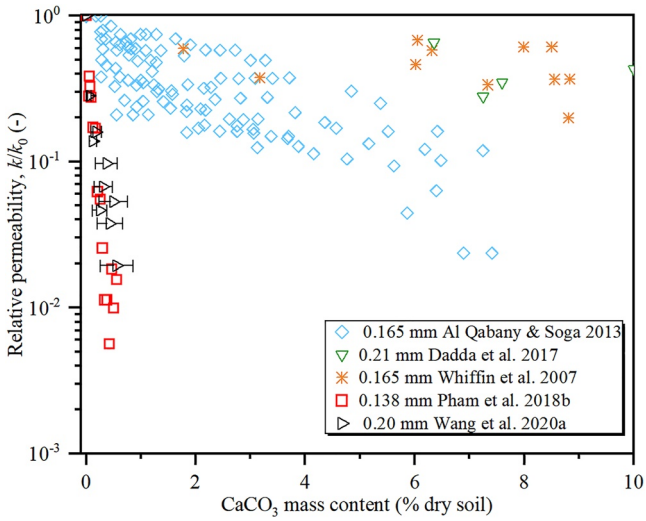


**Figure 6.** Relative permeability change as a function of $CaCO_3$ content for various studies. Al Qabany and Soga (2013), Dadda et al. (2017), and Whiffin et al. (2007) using MICP by urea hydrolysis, which results in $CaCO_3$ precipitation only; Pham, Van Paassen, Van der Star, et al. (2018), and Wang, Van Paassen, et al. (2020) using MIDP (concurrent biogas-biofilm-biomineral formation).

the metabolic growth rate for the data presented by Wang, Van Paassen, et al. (2020). It is hypothesized that at the maximum metabolic growth rate ($f_{cat} = 0.487$), a relatively large amount of biomass fills the pore space, while under catabolic conditions at zero biomass growth ($f_{cat} \rightarrow \infty$) the reduction in porosity is only attributed to the formation of $CaCO_3$. The zero growth (catabolic) and the maximum growth conditions could serve as the permeability development boundaries for MIDP. For the data presented by Pham, Van Paassen, Van der Star, et al. (2018), in which the $f_{cat}$ can be calculated based on the substrate consumption ratio, a factor $\eta$ of 43 provided the best fit.

Compared to the values by Bernabé et al. (2003) and Hommel et al. (2016), these values for $\eta$ are very high for MIDP, which suggests that the combined formation of biogas, biomass and biominerals in the MIDP process leads to efficient clogging, in the sense that only a small amount of products leads to a substantial permeability reduction. To illustrate this clogging efficiency, Figure 6 compares the permeability reduction as a function of $CaCO_3$ content for several studies on biomineralization using MICP by urea hydrolysis (including Al Qabany and Soga (2013), Dadda et al. (2017) and Whiffin et al. (2007)) with MIDP. While the studies based on MICP by urea hydrolysis demonstrated that $CaCO_3$ contents more than 6%–10% were reduce the permeability by one order of magnitude, both studies by Pham, Van Paassen, Van der Star, et al. (2018) and Wang, Van Paassen, et al. (2020) which used MIDP by denitrification reached two orders of magnitude permeability reduction with less than 1% $CaCO_3$.

Similarly, Figure 7 compares the relative change in permeability as a function of the biomass volume ratio from different studies on bio-clogging. The biomass volume ratio is defined as the wet volume of biomass divided by the pore volume. A study by Vandevivere et al. (1995) showed that to reduce the permeability by two orders of magnitude required filling 15%–50% of the pores with biomass, depending on the grain size, which ranged between 0.09 and 0.7 mm. The study by Pham, Van Paassen, Van der Star, et al. (2018) showed that with biomass filling less than 10% of the pores, permeability reduced by more than two orders of magnitude. Including the effect of entrapped gas, the volume fraction of both biomass and gas (considering the volume of $CaCO_3$ is negligibly small) ranges from 20% to 30%, which is more in line with the observations by Vandevivere et al. (1995). It must be noted, as shown in Figure 7, that the reduction in permeability is also affected by the particle size distribution. Still, when comparing only sands with similar median grain size within the range of 0.12–0.21 mm, the reduction in permeability for the MIDP process is still larger compared to the studies on urea hydrolysis or clogging through biomass formation.

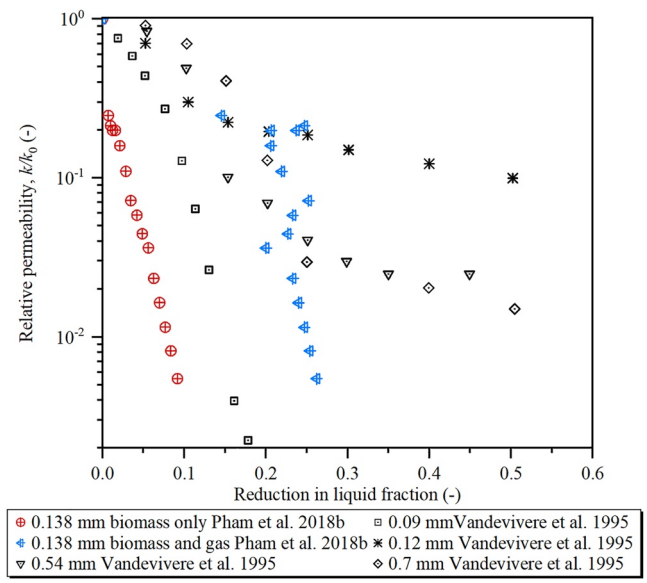


**Figure 7.** Relative permeability reduction as a function of the reduction in liquid fraction reported by Vandevivere et al. (1995) due to biomass only and calculated based on Pham, Van Paassen, Van der Star, et al. (2018) due to biomass only and due to the combination of biomass and biogas.

To explain the observed interaction clogging efficiency in MIDP, we identify three distinct stages in the development of saturation, porosity and permeability as illustrated in Figure 5: (A) non-treated stage; (B) Desaturation dominated stage in which the reduction in permeability is mostly governed by the generation of biogenic gas bubbles within the pores and result in a Pore-filling dominated mechanism; and (C) Biomineral-Biomass Precipitation dominated stage in which the pre-existence of biogenic gas bubbles stimulates the formation of biomineral and biomass in the pore throats (Throat-filling dominated stage) which in turn lead to a significant permeability reduction by even a negligible biomineral or/and biomass formation.

During the initial stages of treatment, liquids can freely flow through the pores and the permeability can be described for the saturated state only (stage A). Even during initial stage of gas formation, the gas bubbles can be

relatively small and freely migrate through the pores. But as the bubbles grow larger to get stuck in the pores and become occluded bubbles and pockets filling the larger pores (stage B). Following the Young-Laplace equation gas pressure is indirectly correlated to the bubble radius, and according to Henry's law it requires a higher concentration to form or maintain gas bubbles in the smaller pores. Consequently, small bubbles tend to dissolve, diffuse, and agglomerate into larger bubbles filling the larger pores first (Mahabadi et al., 2018; Mahabadi & Van Paassen, 2018). As the entrapped gas pockets continue to grow larger than the pores, they start to migrate (preferably upward due to buoyancy) through the pore throats and eventually may form a continuous gas phase. While the gas is filling the larger pores, the liquid is forced to the smaller pores and forms capillary fringes in the pore throats. This would cause more biominerals and biomass to form in or near the smaller pores and narrow pore throats near the particle contacts and consequently could lead to a larger reduction in the permeability (stage C). The precipitation of biominerals and biomass at the pore throats may also reduce the mobility of the gas phase, which could lead to a further and more permanent reduction of the permeability. Cheng et al. (2013) came up with a similar hypothesis as they found that treating sand with MICP by urea hydrolysis in unsaturated conditions lead to higher strengths at similar $CaCO_3$ contents than treatment under saturated conditions. They suggested that MICP treatment under unsaturated conditions, where liquid was only at the capillary fringes surrounding the particle contacts, resulted in more crystals at the particle contacts and thereby more efficient cementation. Also, SEM images provided by O'Donnell, Kavazanjian, and Rittmann (2017) showed smooth rounded, arch-shaped interface of the biominerals, which they attributed to the presence of a gas bubble in the pores. Using pore network model simulations, Nassiri and Mahabadi (2022) demonstrated that the relationships between porosity, saturation and/or permeability can vary significantly depending on the distribution of precipitated minerals and/or gas phase. Comparing simulations with similar $CaCO_3$ content but varying the spatial distribution from a surface coating or a random distribution in the pore bodies to a selectively concentrated precipitates at the pore throats, they demonstrated that the fitting factor $\eta$ or $n$ may range from 2 to over 400.

We expect that the obtained factors $n$ and $\eta$ which were used in the saturation- and porosity-permeability relationships and fitted on the experimental data can vary significantly when used in other experiments, depending on several factors, such as the grain (pore) size distribution of the sand, stratification (Cunningham et al., 1991), the growth rate of the bacteria, substrate consumption rate and bio-mass density. Also, the flow conditions (1D column, 2D plane strain or 3D), flow direction and velocity may affect the distribution of substrates and consequently the distribution of products and resulting permeability relationships (Thullner, 2010). Finally, the experimental set-up and methodology may also affect the actual values. For example, in both studies performed by Pham, Van Paassen, Van der Star, et al. (2018) and Wang, Van Paassen, et al. (2020), the hydraulic conductivity was determined by measuring the head difference between the inlet and outlet tubing where local clogging in the tubing or at the porous stones may have affected the measurements.

## 5. Conclusions

This study evaluated how changes in saturation and porosity affect the permeability during Microbially Induced Desaturation and Precipitation (MIDP) through denitrification. MIDP is a new ground improvement method, in which a solution containing calcium, nitrate and acetate is injected to stimulate indigenous nitrate reducing bacteria to produce biogas, biominerals, and biomass in the soil matrix. A numerical biogeochemical model is developed to evaluate how the combined production of biogas, biominerals, and biomass affects the hydraulic conductivity of the treated soil. The model allows to relate changes in substrate concentration, reaction kinetics, pore pressure, to changes in saturation, porosity, and permeability. Experimental tests reported in the literature were used to calibrate the model and fit the factors defining the reaction stoichiometry and kinetics and the relationships between saturation, porosity, and permeability. The study demonstrated that the combined effects of biogas, biomass and biomineral formation cannot be properly simulated using a single equation describing the relationship between saturation or porosity and permeability. Instead, the effect of desaturation needs to be treated separately from the effect of biomass and biominerals. The numerical analysis of the experimental results also demonstrates that the MIDP process reduces the permeability very efficiently. Permeability was reduced by more than two orders of magnitude at relatively small amount of biomass and biominerals. The clogging efficiency is attributed to the interaction between the three phases.

## Data Availability Statement

The data supporting this paper can be found in the Open Science Framework (OSF), at http://doi.org/10.17605/OSF.IO/NY5GJ. The liquid batch test is simulated with COMSOL Multiphysics® (version 5.3a), available with COMSOL license at https://www.comsol.com.

**Acknowledgments**
This work was supported by the National Science Foundation of China (NSFC) under Grants 52208357 and 52078188, the U.S. National Science Foundation (NSF) Engineering Research Center program under the grant numbered ERC-1449501. Any opinions, findings and conclusions or recommendations expressed in this material are those of the authors and do not necessarily reflect those of the NSF.

## References

Al Qabany, A., & Soga, K. (2013). Effect of chemical treatment used in MICP on engineering properties of cemented soils. *Géotechnique*, *63*(4), 331–339. https://doi.org/10.1680/geot.SIP13.P.022

Baveye, P., Vandevivere, P., Hoyle, B. L., Deleo, P. C., & Sanchez De Lozada, D. (1998). Environmental impact and mechanisms of the biological clogging of saturated soils and aquifer materials. *Critical Reviews in Environmental Science and Technology*, *28*(2), 123–191. https://doi.org/10.1080/10643389891254197

Bernabé, Y., Mok, U., & Evans, B. (2003). Permeability-porosity relationships in rocks subjected to various evolution processes. *Pure and Applied Geophysics*, *160*(5–6), 937–960. https://doi.org/10.1007/PL00012574

Brooks, R. H., & Corey, A. T. (1964). Hydraulic properties of porous media. *Hydrology Papers, Colorado State University*, *3*, 37. Retrieved from https://www.wipp.energy.gov/information_repository/cra/CRA-2014/References/Others/Brooks_Corey_1964_Hydraulic_Properties_ERMS241117.pdf

Chen, C.-Y., & Chen, S.-D. (2000). Biofilm characteristics in biological denitrification biofilm reactors. *Water Science and Technology*, *41*(4–5), 147–154. https://doi.org/10.2166/wst.2000.0438

Cheng, L., Cord-Ruwisch, R., & Shahin, M. A. (2013). Cementation of sand soil by microbially induced calcite precipitation at various degrees of saturation. *Canadian Geotechnical Journal*, *50*(1), 81–90. https://doi.org/10.1139/cgj-2012-0023

Cunningham, A. B., Characklls, W. G., Abedeen, F., & Crawford, D. (1991). Influence of biofilm accumulation on porous media hydrodynamics. *Environmental Science and Technology*, *25*(7), 1305–1311. https://doi.org/10.1021/es00019a013

Cunningham, A. B., Class, H., Ebigbo, A., Gerlach, R., Phillips, A. J., & Hommel, J. (2019). Field-scale modeling of microbially induced calcite precipitation. *Computational Geosciences*, *23*(2), 399–414. https://doi.org/10.1007/s10596-018-9797-6

Cuthbert, M. O., McMillan, L. A., Handley-Sidhu, S., Riley, M. S., Tobler, D. J., & Phoenix, V. R. (2013). A field and modeling study of fractured rock permeability reduction using microbially induced calcite precipitation. *Environmental Science and Technology*, *47*(23), 13637–13643. https://doi.org/10.1021/es402601g

Dadda, A., Geindreau, C., Emeriault, F., Du Roscoat, S. R., Garandet, A., Sapin, L., & Filet, A. E. (2017). Characterization of microstructural and physical properties changes in biocemented sand using 3D X-ray microtomography. *Acta Geotechnica*, *12*(5), 955–970. https://doi.org/10.1007/s11440-017-0578-5

DeJong, J. T., Mortensen, B. M., Martinez, B. C., & Nelson, D. C. (2010). Bio-mediated soil improvement. *Ecological Engineering*, *36*(2), 197–210. https://doi.org/10.1016/j.ecoleng.2008.12.029

DeJong, J. T., Soga, K., Kavazanjian, E., Burns, S., Van Paassen, L., Al Qabany, A., et al. (2013). Biogeochemical processes and geotechnical applications: Progress, opportunities and challenges. *Géotechnique*, *63*(4), 287–301. https://doi.org/10.1680/geot.SIP13.P.017

Doran, P. M. (2013). *Bioprocess engineering principles* (2nd ed.). Elsevier/Academic Press. Retrieved from https://www.sciencedirect.com/book/9780122208515/bioprocess-engineering-principles

Ebigbo, A., Helmig, R., Cunningham, A. B., Class, H., & Gerlach, R. (2010). Modelling biofilm growth in the presence of carbon dioxide and water flow in the subsurface. *Advances in Water Resources*, *33*(7), 762–781. https://doi.org/10.1016/j.advwatres.2010.04.004

Ebigbo, A., Phillips, A., Gerlach, R., Helmig, R., Cunningham, A. B., Class, H., & Spangler, L. H. (2012). Darcy-scale modeling of microbially induced carbonate mineral precipitation in sand columns. *Water Resources Research*, *48*(7), 1–17. https://doi.org/10.1029/2011WR011714

Elmountassir, G., Minto, J. M., Van Paassen, L. A., Salifu, E., & Lunn, R. J. (2018). Applications of microbial processes in geotechnical engineering. In M. G. Geoffrey & S. Sima (Eds.), *Advances in applied microbiology* (Vol. 104, pp. 39–91). Academic Press. https://doi.org/10.1016/bs.aambs.2018.05.001

Gai, X., & Sánchez, M. (2019). An elastoplastic mechanical constitutive model for microbially mediated cemented soils. *Acta Geotechnica*, *14*(3), 709–726. https://doi.org/10.1007/s11440-018-0721-y

Gao, Y., Wang, L., He, J., Ren, J., & Gao, Y. (2022). Denitrification-based MICP for cementation of soil: Treatment process and mechanical performance. *Acta Geotechnica*, *6*(9), 3799–3815. https://doi.org/10.1007/s11440-022-01489-6

Ghezzehei, T. A., Kneafsey, T. J., & Su, G. W. (2007). Correspondence of the Gardner and van Genuchten-Mualem relative permeability function parameters. *Water Resources Research*, *43*(10), W10417. https://doi.org/10.1029/2006WR005339

He, J., & Chu, J. (2014). Undrained responses of microbially desaturated sand under monotonic loading. *Journal of Geotechnical and Geoenvironmental Engineering*, *140*(5), 1–8. https://doi.org/10.1061/(ASCE)GT.1943-5606.0001082

He, J., Chu, J., & Ivanov, V. (2013). Mitigation of liquefaction of saturated sand using biogas. *Géotechnique*, *63*(4), 267–275. https://doi.org/10.1680/geot.SIP13.P.004

He, J., Chu, J., & Liu, H. (2014). Undrained shear strength of desaturated loose sand under monotonic shearing. *Soils and Foundations*, *54*(4), 910–916. https://doi.org/10.1016/j.sandf.2014.06.020

Heijnen, J. J., & Kleerebezem, R. (2009). Bioenergetics of microbial growth. *Encyclopedia of Industrial Biotechnology: Bioprocess, Bioseparation and Cell Technology*, 1–66.

Hoh, C.-Y., & Cord-Ruwisch, R. (1997). Experimental evidence for the need of thermodynamic considerations in modelling of anaerobic environmental bioprocesses. *Water Science and Technology*, *36*(10), 109–115. https://doi.org/10.2166/wst.1997.0370

Hommel, J., Coltman, E., & Class, H. (2018). Porosity–permeability relations for evolving pore space: A review with a focus on (bio-)geochemically altered porous media. *Transport in Porous Media*, *124*(2), 589–629. https://doi.org/10.1007/s11242-018-1086-2

Hommel, J., Lauchnor, E., Gerlach, R., Cunningham, A. B., Ebigbo, A., Helmig, R., & Class, H. (2016). Investigating the influence of the initial biomass distribution and injection strategies on biofilm-mediated calcite precipitation in porous media. *Transport in Porous Media*, *114*(2), 557–579. https://doi.org/10.1007/s11242-015-0617-3

Hommel, J., Lauchnor, E., Phillips, A., Gerlach, R., Cunningham, A. B., Helmig, R., et al. (2015). A revised model for microbially induced calcite precipitation: Improvements and new insights based on recent experiments. *Water Resources Research*, *51*(5), 3695–3715. https://doi.org/10.1002/2014WR016503

Ippisch, O., Vogel, H. J., & Bastian, P. (2006). Validity limits for the van Genuchten-Mualem model and implications for parameter estimation and numerical simulation. *Advances in Water Resources*, *29*(12), 1780–1789. https://doi.org/10.1016/j.advwatres.2005.12.011

Ivanov, V., & Chu, J. (2008). Applications of microorganisms to geotechnical engineering for bioclogging and biocementation of soil in situ. *Reviews in Environmental Science and Biotechnology*, *7*(2), 139–153. https://doi.org/10.1007/s11157-007-9126-3

Ives, K. J., & Pienvichitr, V. (1965). Kinetics of the filtration of dilute suspensions. *Chemical Engineering Science*, *20*(11), 965–973. https://doi.org/10.1016/0009-2509(65)80094-X

Mahabadi, N., & Jang, J. (2014). Relative water and gas permeability for gas production from hydrate-bearing sediments. *Geochemistry, Geophysics, Geosystems*, *15*(6), 2346–2353. https://doi.org/10.1002/2014GC005331

Mahabadi, N., & Van Paassen, L. A. (2018). Pore scale study of gas bubble nucleation and migration in porous media. In *B2G conference*.

Mahabadi, N., Zheng, X., Yun, T. S., Van Paassen, L., & Jang, J. (2018). Gas bubble migration and trapping in porous media: Pore-scale simulation. *Journal of Geophysical Research: Solid Earth*, *123*(2), 1060–1071. https://doi.org/10.1002/2017JB015331

Martinez, B. C., DeJong, J. T., & Ginn, T. R. (2014). Bio-geochemical reactive transport modeling of microbial induced calcite precipitation to predict the treatment of sand in one-dimensional flow. *Computers and Geotechnics*, *58*, 1–13. https://doi.org/10.1016/j.compgeo.2014.01.013

Minto, J. M., Lunn, R. J., & Elmountassir, G. (2019). Development of a reactive transport model for field-Scale simulation of Microbially Induced Carbonate Precipitation. *Water Resources Research*, *55*(8), 7229–7245. https://doi.org/10.1029/2019WR025153

Mualem, Y. (1976). A new model for predicting the hydraulic conductivity of unsaturated porous media. *Water Resources Research*, *12*(3), 513–522. https://doi.org/10.1029/WR012i003p00513

Nassar, M. K., Gurung, D., Bastani, M., Ginn, T. R., Shafei, B., Gomez, M. G., et al. (2018). Large-scale experiments in microbially induced calcite precipitation (MICP): Reactive transport model development and prediction. *Water Resources Research*, *54*(1), 480–500. https://doi.org/10.1002/2017WR021488

Nassiri, S., & Mahabadi, N. (2022). Evolution of porosity–permeability relationships in bio-mediated processes for ground improvement: A pore-scale computational study. In *Geo-congress 2022* (pp. 638–647). American Society of Civil Engineers. https://doi.org/10.1061/9780784484036.064

O'Donnell, S. T. (2016). *Mitigation of earthquake-induced soil liquefaction via microbial denitrification: A two-stage process*. Arizona State University. Retrieved from https://repository.asu.edu/items/38697

O'Donnell, S. T., Hall, C. A., Kavazanjian, E., Rittmann, B. E., O'Donnell, S. T., Hall, C. A., et al. (2019). Biogeochemical model for soil improvement by denitrification. *Journal of Geotechnical and Geoenvironmental Engineering*, *145*(11), 04019091. https://doi.org/10.1061/(ASCE)GT.1943-5606.0002126

O'Donnell, S. T., Kavazanjian, E., & Rittmann, B. E. (2017). Midp: Liquefaction mitigation via microbial denitrification as a two-stage process. II: MICP. *Journal of Geotechnical and Geoenvironmental Engineering*, *143*(12), 04017095. https://doi.org/10.1061/(ASCE)GT.1943-5606.0001806

O'Donnell, S. T., Rittmann, B. E., & Kavazanjian, E. (2017). MIDP: Liquefaction mitigation via microbial denitrification as a two-stage process. I: Desaturation. *Journal of Geotechnical and Geoenvironmental Engineering*, *143*(12), 04017094. https://doi.org/10.1061/(ASCE)GT.1943-5606.0001818

Ohashi, A., & Harada, H. (1994). Characterization of detachment mode of biofilm developed in an attached-growth reactor. *Water Science and Technology*, *30*(11), 35–45. https://doi.org/10.2166/wst.1994.0544

Okamura, M., & Noguchi, K. (2009). Liquefaction resistance of unsaturated non-plastic silt. *Soils and Foundation*, *49*(2), 221–229. https://doi.org/10.3208/sandf.49.221

Okamura, M., & Soga, Y. (2006). Effects of pore fluid compressibility on liquefaction resistance of partially saturated sand. *Soils and Foundations*, *46*(5), 695–700. https://doi.org/10.3208/sandf.46.695

Pham, V. P. (2017). *Bio-based ground improvement through microbial induced desaturation and precipitation (MIDP)*. Delft University of Technology. https://doi.org/10.4233/UUID:3997066A-0AD6-4DE2-9C79-E5E474BAE20F

Pham, V. P., Nakano, A., Van der Star, W. R. L., Heimovaara, T. J., & Van Paassen, L. A. (2018). Applying MICP by denitrification in soils: A process analysis. *Environmental Geotechnics*, *5*(2), 79–93. https://doi.org/10.1680/jenge.15.00078

Pham, V. P., Van Paassen, L. A., & Van der Star, W. R. L. (2018). Quantifying the desaturation effect of biogenic gas formation in sandy soil. In *Proceedings of the 7th International Conference on unsaturated soils. Hongkong*. Retrieved from https://www.researchgate.net/profile/Leon_Van_Paassen/publication/327350722_Quantifying_the_desaturation_effect_of_biogenic_gas_formation_in_sandy_soil/links/5b89a2464585151fd1403500/Quantifying-the-desaturation-effect-of-biogenic-gas-formation-in-sandy-s

Pham, V. P., Van Paassen, L. A., Van der Star, W. R. L., & Heimovaara, T. J. (2018). Evaluating strategies to improve process efficiency of denitrification-based MICP. *Journal of Geotechnical and Geoenvironmental Engineering*, *144*(8), 04018049. https://doi.org/10.1061/(ASCE)GT.1943-5606.0001909

Phillips, A. J., Gerlach, R., Lauchnor, E., Mitchell, A. C., Cunningham, A. B., & Spangler, L. (2013). Engineered applications of ureolytic biomineralization: A review. *Biofouling*, *29*(6), 715–733. https://doi.org/10.1080/08927014.2013.796550

Qin, C. Z., Hassanizadeh, S. M., & Ebigbo, A. (2016). Pore-scale network modeling of microbially induced calcium carbonate precipitation: Insight into scale dependence of biogeochemical reaction rates. *Water Resources Research*, *52*(11), 8794–8810. https://doi.org/10.1002/2016WR019128

Rabah, F. K. J., & Dahab, M. F. (2004). Biofilm and biomass characteristics in high-performance fluidized-bed biofilm reactors. *Water Research*, *38*(19), 4262–4270. https://doi.org/10.1016/j.watres.2004.08.012

Ro, K. S., & Neethling, J. B. (1991). Biofilm density for biological fluidized beds. *Research Journal of the Water Pollution Control Federation*, *63*(5), 815–818.

Ronen, D., Berkowitz, B., & Magaritz, M. (1989). The development and influence of gas bubbles in phreatic aquifers under natural flow conditions. *Transport in Porous Media*, *4*(3), 295–306. https://doi.org/10.1007/BF00138041

Sahimi, M. (1993). Flow phenomena in rocks: From continuum models to fractals, percolation, cellular automata, and simulated annealing. *Reviews of Modern Physics*, *65*(4), 1393–1534. https://doi.org/10.1103/RevModPhys.65.1393

Şengör, S. S., Ginn, T. R., Brugato, C. J., & Gikas, P. (2013). Anaerobic microbial growth near thermodynamic equilibrium as a function of ATP/ADP cycle: The effect of maintenance energy requirements. *Biochemical Engineering Journal*, *81*, 65–72. https://doi.org/10.1016/j.bej.2013.10.006

Soares, M. I. M., Belkin, S., & Abeliovich, A. (1988). Biological groundwater denitrification: Laboratory studies. *Water Science and Technology*, *20*(3), 189–195. https://doi.org/10.2166/wst.1988.0098

Soares, M. I. M., Braester, C., Belkin, S., & Abeliovich, A. (1991). Denitrification in laboratory sand columns: Carbon regime, gas accumulation and hydraulic properties. *Water Research*, *25*(3), 325–332. https://doi.org/10.1016/0043-1354(91)90013-G

Stallings Young, E. G., Mahabadi, N., Zapata, C. E., & Van Paassen, L. A. (2021). Microbial-Induced Desaturation in stratified soil conditions. *International Journal of Geosynthetics and Ground Engineering*, *7*(2), 37. https://doi.org/10.1007/s40891-021-00276-9

Stone, H. L. (1970). Probability model for estimating three-phase relative permeability. *Journal of Petroleum Technology*, *22*(02), 214–218. https://doi.org/10.2118/2116-PA

Thomsen, J. K., Geest, T., & Cox, R. P. (1994). Mass spectrometric studies of the effect of pH on the accumulation of intermediates in denitrification by *Paracoccus denitrificans*. *Applied and Environmental Microbiology*, *60*(2), 536–541. https://doi.org/10.1128/aem.60.2.536-541.1994

Thullner, M. (2010). Comparison of bioclogging effects in saturated porous media within one- and two-dimensional flow systems. *Ecological Engineering*, *36*(2), 176–196. https://doi.org/10.1016/j.ecoleng.2008.12.037

Vandevivere, P. (1995). Bacterial clogging of porous media: A new modelling approach. *Biofouling*, *8*(4), 281–291. https://doi.org/10.1080/08927019509378281

Vandevivere, P., Baveye, P., De Lozada, D. S., & DeLeo, P. (1995). Microbial clogging of saturated soils and aquifer materials: Evaluation of mathematical models. *Water Resources Research*, *31*(9), 2173–2180. https://doi.org/10.1029/95WR01568

Van Genuchten, M. T. (1980). A closed-form equation for predicting the hydraulic conductivity of unsaturated soils. *Soil Science Society of America Journal*, *44*(5), 892–898. https://doi.org/10.2136/sssaj1980.03615995004400050002x

Van Paassen, L. A. (2009). *Biogrout, ground improvement by microbial induced carbonate precipitation*. Delft University of Technology. Retrieved from https://www.narcis.nl/publication/RecordID/oai:tudelft.nl:uuid:5f3384c4-33bd-4f2a-8641-7c665433b57b

Van Paassen, L. A., Daza, C. M., Staal, M., Sorokin, D. Y., Van der Zon, W., & Van Loosdrecht, M. C. M. (2010). Potential soil reinforcement by biological denitrification. *Ecological Engineering*, *36*(2), 168–175. https://doi.org/10.1016/j.ecoleng.2009.03.026

Van Paassen, L. A., Pham, V. P., Mahabadi, N., Hall, C., Stallings, E., & Kavazanjian, E. (2018). Desaturation via biogenic gas formation as a ground improvement technique. In *PanAm unsaturated soils 2017* (pp. 244–256). American Society of Civil Engineers. https://doi.org/10.1061/9780784481677.013

Van Wijngaarden, W. K., Van Paassen, L. A., Vermolen, F. J., Van Meurs, G. A. M., & Vuik, C. (2016). A reactive transport model for biogrout compared to experimental data. *Transport in Porous Media*, *111*(3), 627–648. https://doi.org/10.1007/s11242-015-0615-5

Van Wijngaarden, W. K., Vermolen, F. J., Van Meurs, G. A. M., & Vuik, C. (2011). Modelling biogrout: A new ground improvement method based on microbial-induced carbonate precipitation. *Transport in Porous Media*, *87*(2), 397–420. https://doi.org/10.1007/s11242-010-9691-8

Van Wijngaarden, W. K., Vermolen, F. J., Van Meurs, G. A. M., & Vuik, C. (2013). A mathematical model for biogrout: Bacterial placement and soil reinforcement. *Computational Geosciences*, *17*(3), 463–478. https://doi.org/10.1007/s10596-012-9316-0

Verma, A., & Pruess, K. (1988). Thermohydrological conditions and silica redistribution near high-level nuclear wastes emplaced in saturated geological formations. *Journal of Geophysical Research*, *93*(B2), 1159–1173. https://doi.org/10.1029/JB093iB02p01159

Wang, L., Gao, Y., He, J., Gao, Y., & Van Paassen, L. A. (2021). Effect of biogenic gas formation through Microbial Induced Desaturation and Precipitation on the static response of sands with varied relative density. *Journal of Geotechnical and Geoenvironmental Engineering*, *147*(8), 04021071. https://doi.org/10.1061/(ASCE)GT.1943-5606.0002578

Wang, L., Van Paassen, L., Gao, Y., He, J., Gao, Y., & Kim, D. (2020). Laboratory tests on mitigation of soil liquefaction using microbial induced desaturation and precipitation. *Geotechnical Testing Journal*, *44*(2), 520–534. https://doi.org/10.1520/GTJ20190432

Wang, L., Van Paassen, L. A., & Kavazanjian, E. (2020). Feasibility study on liquefaction mitigation of Fraser river sediments by microbial induced desaturation and precipitation (MIDP). *GeoCongress*, *2020*, 121–131. https://doi.org/10.1061/9780784482834.014

Whiffin, V. S., Van Paassen, L. A., & Harkes, M. P. (2007). Microbial carbonate precipitation as a soil improvement technique. *Geomicrobiology Journal*, *24*(5), 417–423. https://doi.org/10.1080/01490450701436505

Wu, S., Li, B., He, J., & Chu, J. (2018). Biogeotechnological methods for mitigation of liquefaction. *Geotechnical Engineering*, *49*(1), 143–149.

Zeng, C., Veenis, Y., Hall, C. A., Young, E. S., Van der Star, W. R. L., Zheng, J., & Van Paassen, L. A. (2021). Experimental and numerical analysis of a field trial application of Microbially Induced Calcite Precipitation for ground stabilization. *Journal of Geotechnical and Geoenvironmental Engineering*, *147*(7), 05021003. https://doi.org/10.1061/(asce)gt.1943-5606.0002545

Zhan, X. M., Rodgers, M., & O'Reilly, E. (2006). Biofilm growth and characteristics in an alternating pumped sequencing batch biofilm reactor (APSBBR). *Water Research*, *40*(4), 817–825. https://doi.org/10.1016/j.watres.2005.12.003